Annals of Glaciology

Distributed energy balance, mass balance and climate sensitivity of upper Chandra Basin glaciers, western Himalaya

Sunil N. Oulkar[1], Parmanand Sharma[1], Bhanu Pratap[1], Meloth Thamban[1], Sourav Laha[1], Lavkush Kumar Patel[1,2] and Ajit T. Singh[1]

[1]National Centre for Polar and Ocean Research, Ministry of Earth Sciences, Vasco-da-Gama Goa, 403804, India. and [2]National Institute of Hydrology, Roorkee, Uttarakhand, 247667, India

Article

Cite this article: Oulkar SN, Sharma P, Pratap B, Thamban M, Laha S, Patel LK, Singh AT (2025) Distributed energy balance, mass balance and climate sensitivity of upper Chandra Basin glaciers, western Himalaya. *Annals of Glaciology* **66**, e5, 1–12. https://doi.org/10.1017/aog.2024.46

Received: 3 July 2024
Revised: 21 November 2024
Accepted: 2 December 2024

Keywords:
climate sensitivity; energy and mass balance; upper Chandra Basin; western Himalaya

Corresponding author: Parmanand Sharma; Email: pnsharma@ncpor.res.in

Abstract

Glacier and snow melt are the primary sources of water for streams, and rivers in upper Indus region of the western Himalaya. However, the magnitude of runoff from this glacierized basin is expected to vary with the available energy in the catchment. Here, we used a physically based energy balance model to estimate the surface energy and surface mass balance (SMB) of the upper Chandra Basin glaciers for 7 hydrological years from 2015 to 2022. A strong seasonality is observed, with net radiation being the dominant energy flux in the summer, while latent and sensible heat flux dominated in the winter. The estimated mean annual SMB of the upper Chandra Basin glaciers is -0.51 ± 0.28 m w.e. a^{-1}, with a cumulative SMB of −3.54 m w.e during 7 years from 2015 to 2022. We find that the geographical factors like aspect, slope, size and elevation of the glacier contribute towards the spatial variability of SMB within the study region. The findings reveal that a 42% increase in precipitation is necessary to counteract the additional mass loss resulting from a 1°C increase in air temperature for the upper Chandra Basin glaciers.

1. Introduction

The Himalayan region extends over eight countries across Asia (Afghanistan, Bangladesh, Bhutan, China, India, Myanmar, Nepal and Pakistan) and is home to the world's largest ice volume outside the polar regions (Bolch, 2012). These are often called the 'Water Tower of Asia', emphasizing their immense importance as a freshwater resource (Immerzeel, 2020). The meltwater from Himalayan glaciers plays a crucial role in supporting hydropower generation, irrigation and the essential needs of the human population and natural ecosystems (Pritchard, 2019; Immerzeel, 2020; Li, 2022). However, over the past few decades, these glaciers have experienced substantial mass loss (Kaab and others, 2012). Due to the high elevation and challenging terrain of the Himalayas, scientific studies in this region are limited, resulting in gaps in our understanding of various factors including atmospheric conditions, energy fluxes, glacier–atmosphere interaction and glacier dynamics (Mayewski and others, 2020). In particular, calibration and validation of model studies are scarce and filling these knowledge gaps would reduce uncertainty in climate change projections.

The Himalayan region has complex climatic conditions due to the influences of the Indian Summer Monsoon (ISM) system and Western Disturbances (WD), which cause variability in meteorological conditions over the area (Bolch, 2012; Hock and others, 2019; Azam, 2021). In addition, the heterogeneous changes in glacier mass balance are driven primarily by mechanisms associated with altitude-dependent warming, surrounding topography, land–atmospheric interactions and seasonal to interannual variation in atmospheric circulations on a large or regional scale (Kulkarni, 2007; Pepin, 2022; Nair and others, 2023). The higher temperature increases the fraction of solid to liquid precipitation and reduces accumulation (Wang and others, 2013). Further, it intensifies the melt and lengthens the ablation season duration (Arndt and Schneider, 2023). Rising snowlines expose more glacier ice, reducing surface albedo and leading to further melt through snow-albedo feedback (Bolch, 2012). Warming can also alter meltwater refreezing, retention, surface roughness and glacier flow dynamics (Sakai and Fujita, 2017). All these processes interact to change glacier surface energy balance (SEB) and surface mass balance (SMB). Therefore, it is essential to understand the response of glaciers to atmospheric forcing using hydrometeorological observations and numerical models.

To adequately capture the full SEB and SMB, a distributed physically based model incorporating spatial variability in meteorological conditions and surface properties is required (Hock and Holmgren, 2005). Ablation processes are governed by the SEB, consisting of radiative fluxes (net shortwave and longwave radiation), turbulent fluxes (latent and sensible heat), latent heat flux from rain and heat conduction into the snow/ice. The heterogeneity of glaciers and their surrounding topography creates significant spatial variability in meteorological variables, leading to complex patterns in energy and mass fluxes (Yu, 2013; Brun, 2019; Patel, 2021). Physically based model studies have demonstrated the importance of implementing distributed approaches to capture the substantial variations in SMB across glaciers (Reijmer and others, 2012). The Western Himalaya, particularly the Chandra Basin in the upper Indus Basin, is an important region for studying glaciers, as it contains several glaciers that are experiencing significant mass loss (Gardelle and others, 2013; Vijay and Braun, 2016; Sharma and others, 2020; Patel, 2021; Pratap, 2023). However, only a few studies from this region have high-resolution data focusing on the variability of meteorological parameters and energy fluxes, limiting our understanding of glacier–atmosphere interactions.

In this study, we have investigated and quantified the distributed SEB and SMB of the upper Chandra Basin glaciers for 7 hydrological years from 2015 to 2022 to understand how glacier SMB is affected by climatic (meteorological variability) and non-climatic (topographic characteristics) factors. In this study, we apply the COSIPY model (COupled Snowpack and Ice SEB and mass-balance model in PYthon) (Sauter and others, 2020) to simulate the SEB and SMB of selected glaciers. There are four automatic weather stations (AWS) located within the study area which are in close proximity to the glaciers, one AWS is situated on the glacier, while the other three are located within ∼3 km distance. The data obtained from these AWS are used to extrapolate the hourly meteorological variables across the glacier surface, combined with a resampled digital elevation model (DEM), to derive the spatial distribution of SEB and SMB. Furthermore, the model is calibrated using in situ point SMB measurements and then validated over Sutri Dhaka Glacier and Samudra Tapu Glacier. Sources of uncertainty related to meteorological forcing, model parameters and surface characteristics are quantified through Monte Carlo analysis. Furthermore, we analysed both climatic and non-climatic factors influencing the SMB of glaciers in the study region. The sensitivity of glacier SMB to climatic variations is crucial, and therefore, we conducted perturbation experiments to assess the impacts of changes in air temperature and precipitation.

2. Study area

The Chandra Basin is one of the major sub-basins of the Chenab River within the Indus River system, which is located in the central crystalline axis of the Pir Panjal range in Lahaul-Spiti, Himachal Pradesh, India (Fig. 1). The Chandra River originates from the southern slopes of the Baralacha Pass and flows for ∼125 km through the basin before joining the Bhaga River at Tandi (Fig. 1). The Chandra Basin covers a geographical area of 2446 km^2. The elevation ranges from 2800 to 6592 m a.s.l. and the mean slope is ∼26°. It has 211 glaciers, covering an area of 631 km^2 (∼26% of the total basin area) (Fig. 1). The basin is located within the transition zone between monsoon and arid climate and experiences the ISM during summer (July–September) and the Northern Hemisphere Mid Latitude WD during winter (December–April) (Bookhagen and Burbank, 2010). However, ∼60–80% of the annual precipitation occurs during the winter mainly in the form of snowfall, whereas the remaining 20–40% falls during the summer monsoon season (Koul and Ganjoo, 2010; Oulkar, 2022).

The Chandra Basin glaciers have large differences in size, surface characteristics and orientation/aspect (Fig. 1b). A significant variability in the SEB, particularly the net shortwave radiation within the basin, is caused by both non-climatic and climatic parameters (Patel, 2021; Oulkar, 2022). Therefore, we have categorized the glaciers in the upper Chandra Basin based on the orientation and size of the glaciers (Fig. 1c). The selected glaciers in the upper Chandra Basin are mostly oriented towards the northeast, south and southwest, which has been valuable for conducting orientation analysis. In contrast, the remaining glaciers exhibit substantial variation in orientation, and including these glaciers would have increased the computational time and complexity of the analysis. The selected glaciers cover an area of ∼298 km^2, ∼47% of the total glacierized area of the Chandra Basin. In the present study, we have considered only those glaciers which cover an area ≥1 km^2, a criterion employed to mitigate uncertainties and ensure a more precise examination of the glacier SEB and SMB. In addition, all these selected glaciers are debris-free glaciers and partially covered with debris over the lower ablation zone. Within the catchment of this study region, we have four AWS installed to monitor the hydrometeorological conditions (Fig. 1 and Fig. S1 in the Supplementary). One AWS is situated on the glacier, while the other three are located within a distance of 3 km. The study area covers 18 glaciers in the upper Chandra Basin which also include benchmark glaciers such as Samudra Tapu and Sutri Dhaka. We have in situ SMB measurements for Sutri Dhaka Glacier and Samudra Tapu Glacier from 2015 to 2022 (Fig. S3 in the Supplementary). These in situ observations are used to validate and estimate the uncertainty of modelled SMB. This will significantly strengthen the effectiveness of the SEB and SMB model simulation and offer a fast and efficient method to evaluate the model performance.

3. Data collection and methodology

3.1. Meteorological data

The locations and elevations of each AWS are provided in Figure S1 and Table S1. The AWS network includes various meteorological sensors connected to Campbell CR1000 and CR1000X data loggers stored within watertight enclosures. The sensor specifications, accuracy and meteorological variables are detailed in Table 1. The sensors collect data at intervals of 10 min, 30 min and daily, which are stored by the data logger and retrieved during field expeditions. The quality control checks applied to the AWS data include a range test to identify values outside acceptable ranges, an internal consistency test, a time series consistency test to detect sudden jumps or spikes in the data and a spatial consistency test, which involves cross-referencing data with nearby stations to ensure data consistency (Estévez and others, 2011). Additionally, outliers were identified using statistical analysis, such as detecting values beyond 3 SD from the mean (Estévez and others, 2011).

To estimate the SEB and SMB of the glaciers in the upper Chandra Basin, we used hourly meteorological data from the Himansh Base Camp (HBC) AWS located at 4052 m elevation. The HBC has the longest data from October 2015 to September 2022 with only minor data gaps owing to power cuts compared to other AWS (Table S1 in the Supplementary). To fill the data gap, we have used hourly data which has a spatial resolution of 0.1° × 0.1°, obtained from the European Centre for Medium-Range Weather Forecasts reanalysis (ERA5-land: https://cds.climate.copernicus.eu/cdsapp#!/dataset/reanalysis-era5-land?tab=overview) (Hersbach, 2020) at the nearest surface grid points of HBC AWS using bias correction. The bias correction method involved

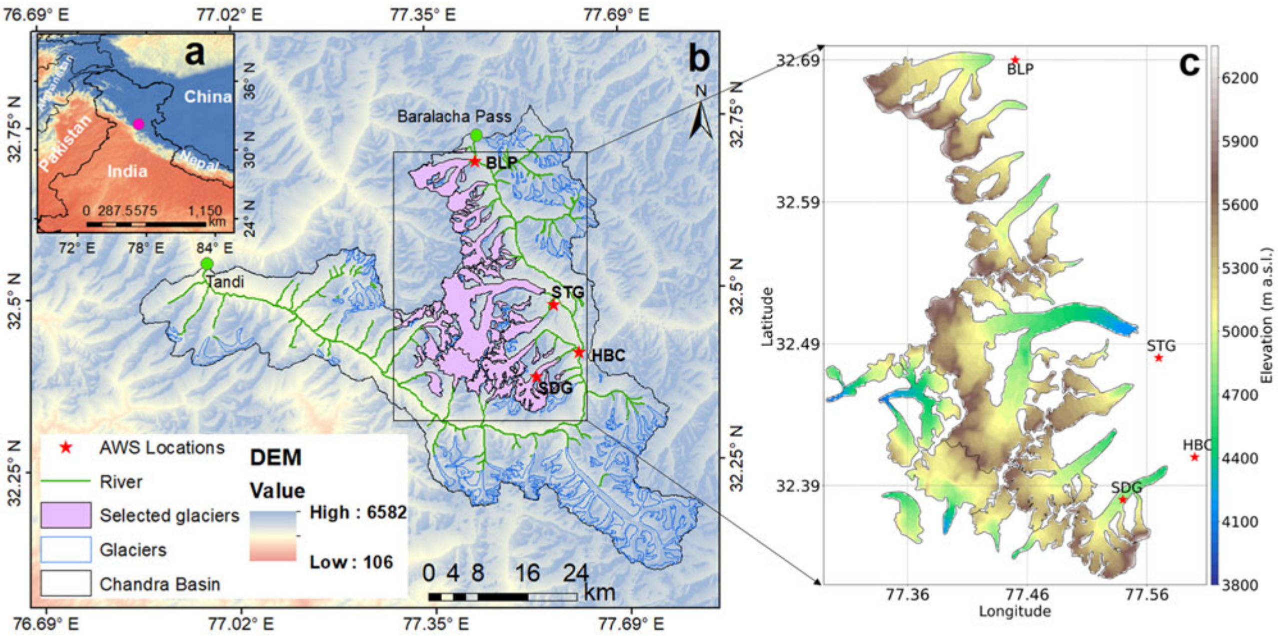

Figure 1. Location map (a) of the study region in the western Himalaya, (b) the Chandra Basin with selected glaciers (pink colour) and (c) elevation gradient of the selected glaciers. The red star represents automatic weather stations (AWS); Himansh Base Camp (HBC, 4052 m a.s.l.), Sutri Dhaka Glacier (SDG, 4864 m a.s.l.), Samudra Tapu Glacier (STG, 4513 m a.s.l.) and Baralacha Pass (BLP, 4904 m a.s.l.).

Table 1. List of the AWS sensors and parameters used in the study

Parameter	Sensor type	Measurement range	Sensor accuracy	Height from the surface (m)
Air temperature	Campbell HC2S3	−50°C to +60°C	±0.1°C	2
Relative humidity	Campbell HC2S3	0–100% RH	±0.8% RH	2
Wind speed & wind direction	RM Young Sensor 05103	0–100 ms^{-1}	±0.3 ms^{-1} & ±3° direction	4
Solar radiation (incoming & outgoing)	Kipp & Zonen CNR4	0–2000 Wm^{-2}	± 10%-day total	4
Longwave radiation (incoming & outgoing)	Kipp & Zonen CNR4		± 10%-day total	4
Precipitation	OTT Pluvio^2	12–1800 mm/h	± 0.05 mm	0
Air pressure	Vaisala CS106	500–1100 hPa	±1.5 hPa (−40 to +60°C)	2

fine-tuning the ERA5-l and reanalysis data using a linear regression model to align with the observed data from the HBC AWS (Maraun and Widmann, 2018). We calculated the bias by comparing the reanalysis data with the observed data during overlapping periods and applied a correction factor based on the SD. This statistical adjustment ensured that the corrected data closely matched the characteristics of the observed data, improving the accuracy of the gap-filled data. Cloud cover over the study area is estimated using the method from Van den Broeke and others (2006). This method calculates cloud cover as a fraction between 0 and 1 based on net longwave radiation and air temperature measurements.

To simulate the SEB and SMB of the selected glaciers, we use a 100 m resolution DEM derived from the 30 m ASTER GDEM V2 dataset. The ASTER GDEM V2 data are obtained from the Earth Remote Sensing Data Analysis Centre (ERSDAC) (Tachikawa, 2011). The lapse rate/vertical gradient is highly sensitive to surface characteristics and local microclimate, and thus significant variations are expected in the extrapolated data. To ensure accurate distributed data, we have partitioned the selected upper Chandra Basin glaciers into four zones: CB1, CB2, CB3 and CB4 (Fig. S2 in the Supplementary). This division is based on the proximity of these zones to four installed AWS (HBC, STG-Samudra Tapu Glacier, SDG-Sutri Dhaka Glacier and BLP-Baralacha Pass) (Fig. S2 in the Supplementary). Meteorological data obtained from these AWS are utilized to estimate lapse rates for the corresponding zones, thereby representing the vertical gradients of air temperature and relative humidity (Table S1 in the Supplementary). Lapse rates are computed on a mean annual basis by regression of the AWS data against station elevation for the common observation period of AWS data. The lapse rates are then applied to extrapolate the point HBC AWS data to the entire DEM based on the elevation at each 100 m grid cell to obtain distributed SEB and SMB of the glaciers (Table 2). The precipitation and air pressure gradient data used in this analysis are obtained from previous study by Oulkar (2022). These distributed meteorological data are used as inputs to the SEB model to simulate hourly SMB for the 7 hydrological years.

3.2. *Methodology*

We have used the COSIPY model, which is an open-source (https://github.com/cryotools/cosipy), physically based model that simulates the SEB, SMB and subsurface processes for glaciers (Sauter and others, 2020). The model is based on energy and mass conservation and estimates of SEB and SMB. It combines a SEB model with a multilayer snow and ice model to calculate energy fluxes, subsurface processes and SMB at a given resolution (Huintjes, 2015; Sauter and others, 2020). For the present study, the model is forced with HBC AWS hourly observations of incoming

Table 2. Details of model parameters (altitudinal gradient/lapse rates) and extrapolation methods

	Parameters/Model			
Variables	CB1	CB2	CB3	CB4
Air temperature lapse rate (°C m^{-1})	−0.0035	−0.0031	−0.0044	−0.0037
Relative humidity lapse rate (% m^{-1})	0.049	0.032	0.022	0.031
Precipitation gradient (% m^{-1})	0.12 (Oulkar, 2022)			
Air pressure gradient (hPa m^{-1})	−0.034 (Oulkar, 2022)			
Cloud covers	Estimated based on *Lnet* and *Tair* (Van den Broeke and others, 2006)			
Incoming shortwave radiation	Solar radiation model (Georg and others, 2016)			
Longwave radiation	Stefan–Boltzmann law (Klok and Oerlemans, 2002)			
DEM: digital elevation model (m)	100 × 100 m resolution			

Details of CB1, CB2, CB3 and CB4 are given in Fig. S2 in the Supplementary. The air temperature and relative humidity lapse rates are computed for the common observation period from October 2020 to September 2022 using data from all AWS.

shortwave radiation, incoming longwave radiation, air temperature, total precipitation, relative humidity, surface pressure, wind speed and cloud cover fraction during 2015–22.

3.2.1. SEB model

Hourly HBC AWS data and 100 m DEM are used for the COSIPY model to derive the spatial distribution of SEB and SMB of the upper Chandra Basin. The total surface energy flux (Wm^{-2}) at the glacier surface is calculated within the COSIPY model at each time step (hourly) for each grid based on the principle of energy conservation (Oerlemans, 2001):

$$Q = S_{\mathrm{in}}\,(1-\alpha) + L_{\mathrm{in}} + L_{\mathrm{out}} + H_{\mathrm{se}} + H_{\mathrm{la}} + Q_{\mathrm{G}} \tag{1}$$

where Q is the total energy available for melt, S_{in} is the incoming shortwave radiation, α is the surface albedo, L_{in} is the incoming longwave radiation, L_{out} is the outgoing longwave radiation, H_{se} is the turbulent sensible heat flux, H_{la} is the turbulent latent heat flux and Q_{G} is the ground heat flux. The heat flux resulting from liquid precipitation has a negligible effect; therefore, it is not considered in the model (Huintjes, 2015; Sauter and others, 2020; Oulkar, 2022). The sign convention for the energy flux terms is that the positive values represent an energy gain from the surface, while negative values represent an energy loss from the surface. Here, Q is determined through an iteration using a Newton–Raphson optimization scheme to solve the SEB equation (Sauter and others, 2020). The surface temperature is the primary variable associated with the energy fluxes. If the resultant surface temperature exceeds 0°C, the excess energy is available for melt ($Q > 0$) and the surface temperature is reset to 0°C.

The S_{in} is modelled using the approach of Georg and others (2016) which accounts for the effects of topographic shading, slope and aspect on the solar radiation received at the glacier surface. The decrease of S_{in} through the snowpack is computed using an exponential extinction function based on depth, with separate coefficients for snow and ice (Sauter and others, 2020). The surface α is calculated as a function of snowfall, snow depth, snow age and ice albedo following Oerlemans and Knap (1998). The albedo decreases exponentially from fresh snow to firn albedo over a period of 6 days (Huintjes, 2015; Sauter and others, 2020). The surface albedo parameters in our model are set based on the values determined by Molg and Scherer (2012). The Stefan–Boltzmann law is used to estimate the modelled L_{out} (Klok and Oerlemans, 2002). The turbulent heat fluxes (sensible and latent) are computed using the bulk aerodynamic method with stability corrections, based on measurements of air temperature, humidity and wind speed at 2 m above the surface (Oerlemans, 2001). Stability corrections for stratification are included based on the bulk Richardson number. The surface roughness length for momentum, heat and moisture transfer evolve from fresh snow to ice values based on time or snow depth (Sauter and others, 2020). The Q_{G} is comprised of heat conduction fluxes combined with fluxes from the portion of shortwave radiation that penetrates the snowpack/ice.

The values of site-specific parameters within the model are taken from previous studies (Klok and Oerlemans, 2002; Huintjes, 2015; Oulkar, 2022) for SEB and SMB simulations at the upper Chandra Basin glaciers. The air temperature and relative humidity lapse rates are estimated within the present study, while precipitation and air pressure gradients are adopted from Oulkar (2022) (Table 2). Further, the subsurface density profile is initialized on 1 October with constant densities of 870 kg m^{-3} for glacier ice and 490 kg m^{-3} for snow, based on values used in previous studies (Oulkar, 2022; Pratap and others, 2019).

3.2.2. SMB model

The SMB is estimated as follows:

$$\mathrm{SMB} = \mathrm{Ab} + \mathrm{Ac} + \mathrm{Aci} + \mathrm{Abi} \tag{2}$$

where Ab is the surface ablation from melt and sublimation, Ac is an accumulation from snowfall and deposition, Aci is the internal accumulation from refreezing and Abi is the internal ablation from subsurface melt. Solid precipitation (snowfall) contributes directly to accumulation. Liquid precipitation (rainfall) and meltwater percolate through the snowpack following a tipping bucket approach based on the liquid water holding capacity (Sauter and others, 2020). Refreezing occurs when snow temperature is below 0°C and liquid water is present from rainfall or melt. Excess meltwater that reaches the bottom of the snowpack contributes to runoff. The model uses a dynamic mesh with variable layering to represent the vertical profile of snow and ice properties, including temperature, density, liquid water content and ice fraction (Sauter and others, 2020). Layer thickness adapts over time, with thinner layers near the surface and increasing thickness with depth. For more information, the COSIPY model is described in detail by Sauter and others (2020), including the parametrizations, underlying physical principles, model structure and optimization approach.

3.2.3. Model uncertainty assessment

The uncertainty in the model output comes from different sources, such as measurements of meteorological variables, uncertainty of energy fluxes, model parameters, threshold values, etc. Therefore, to assess model uncertainty, we perform 500 Monte Carlo simulations varying model parameters and thresholds by 10% and meteorological inputs within measurement uncertainty ranges, following van der Veen (2002) and Machguth and others (2008). Model uncertainty is quantified by running the repeated simulations at all observed point locations on Samudra Tapu Glacier and Sutri Dhaka Glacier (Fig. S3 in the Supplementary). The mean SMB of 500 Monte Carlo simulations is within the uncertainty range of the corresponding in situ values. Based on the results of the 500 simulations compared against the observed SMB, there is a well match between the uncertainty range and observed SMB (Fig. S4 in

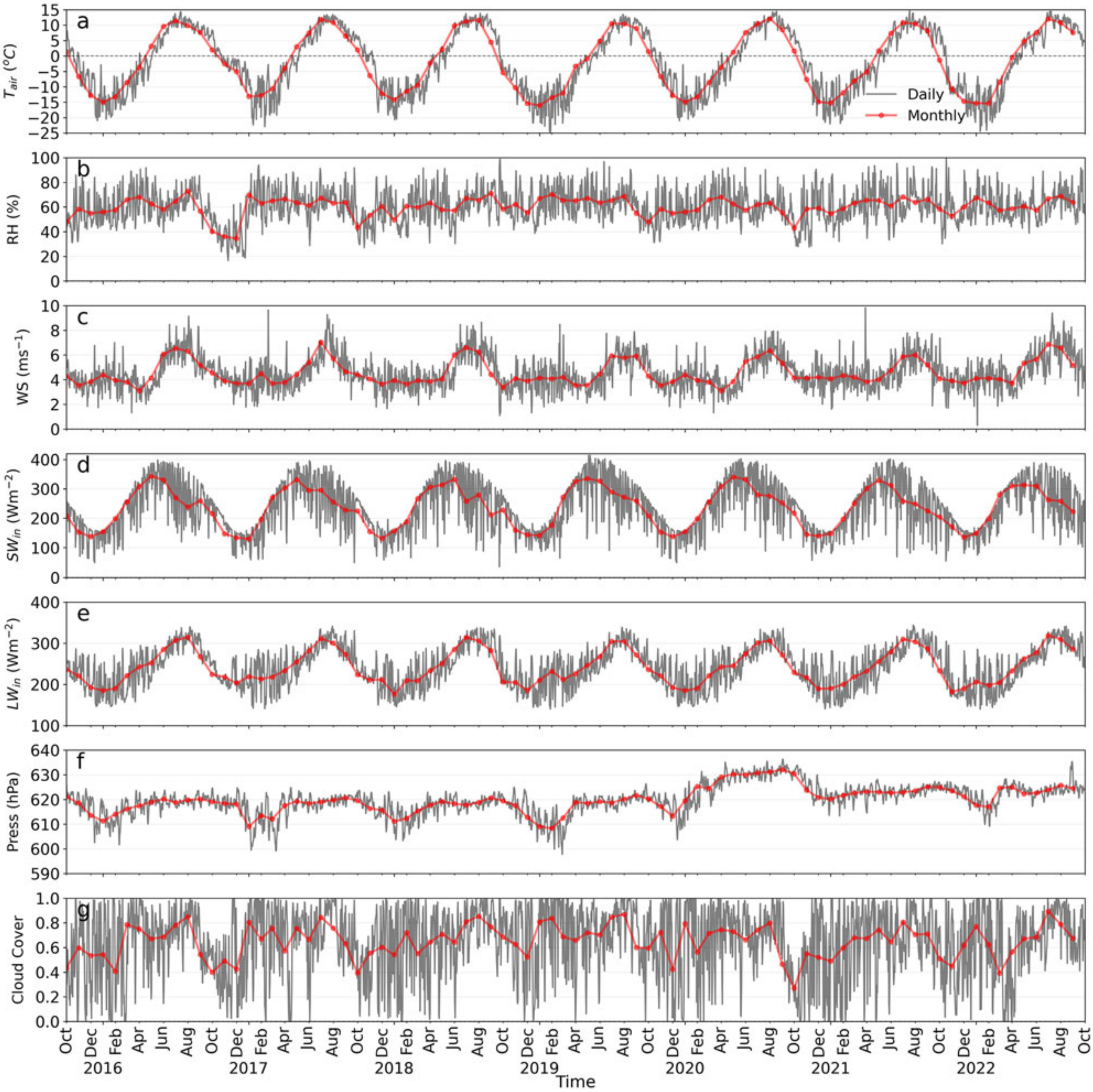

Figure 2. Observed daily mean values of (a) air temperature (T_{air}, °C), (b) relative humidity (RH, %), (c) wind speed (m s^{-1}), (d) incoming shortwave radiation (SW_{in}, Wm^{-2}), (e) incoming longwave radiation (LW_{in}, Wm^{-2}), (f) pressure (hPa), and (g) cloud cover over the Chandra Basin glaciers at the site HBC AWS for study period from October 2015 to September 2022.

the Supplementary). This uncertainty range is determined by calculating the SD of the SMB results. The SD captures the spread in SMB estimates from the 500 simulations. With a normal distribution of results, ~68% of simulations are within $\pm1\sigma$. Therefore, the $\pm$25% uncertainty range represents $\sim\pm1\sigma$ of the SMB results from the simulations.

4. Results and discussion

4.1. Climatic setting

Figure 2 shows the observed daily mean values of air temperature, surface temperature, relative humidity, wind speed, cloud cover, air pressure, incoming shortwave and incoming longwave radiation over the upper Chandra Basin glaciers for the study period from October 2015 to September 2022. These meteorological variables show substantial temporal variation and distinct patterns over the study period. The daily mean air temperature ranges from −25.48°C to 15.67°C with a mean annual value of 1.67°C (Fig. 2a). The daily mean relative humidity ranges from 16% to 99%, with a mean annual value of 60% (Fig. 2b). The daily mean wind speed ranges from 0 to 9.84 m s^{-1} with a mean annual value of 4.57 m s^{-1} (Fig. 2c). The daily mean incoming shortwave radiation ranges from 37 to 400 Wm^{-2} with a mean annual value of 237 Wm^{-2} (Fig. 2d). The incoming longwave radiation ranges from 139 to 344 Wm^{-2} with a mean annual value of 243 Wm^{-2} (Fig. 2e). The daily

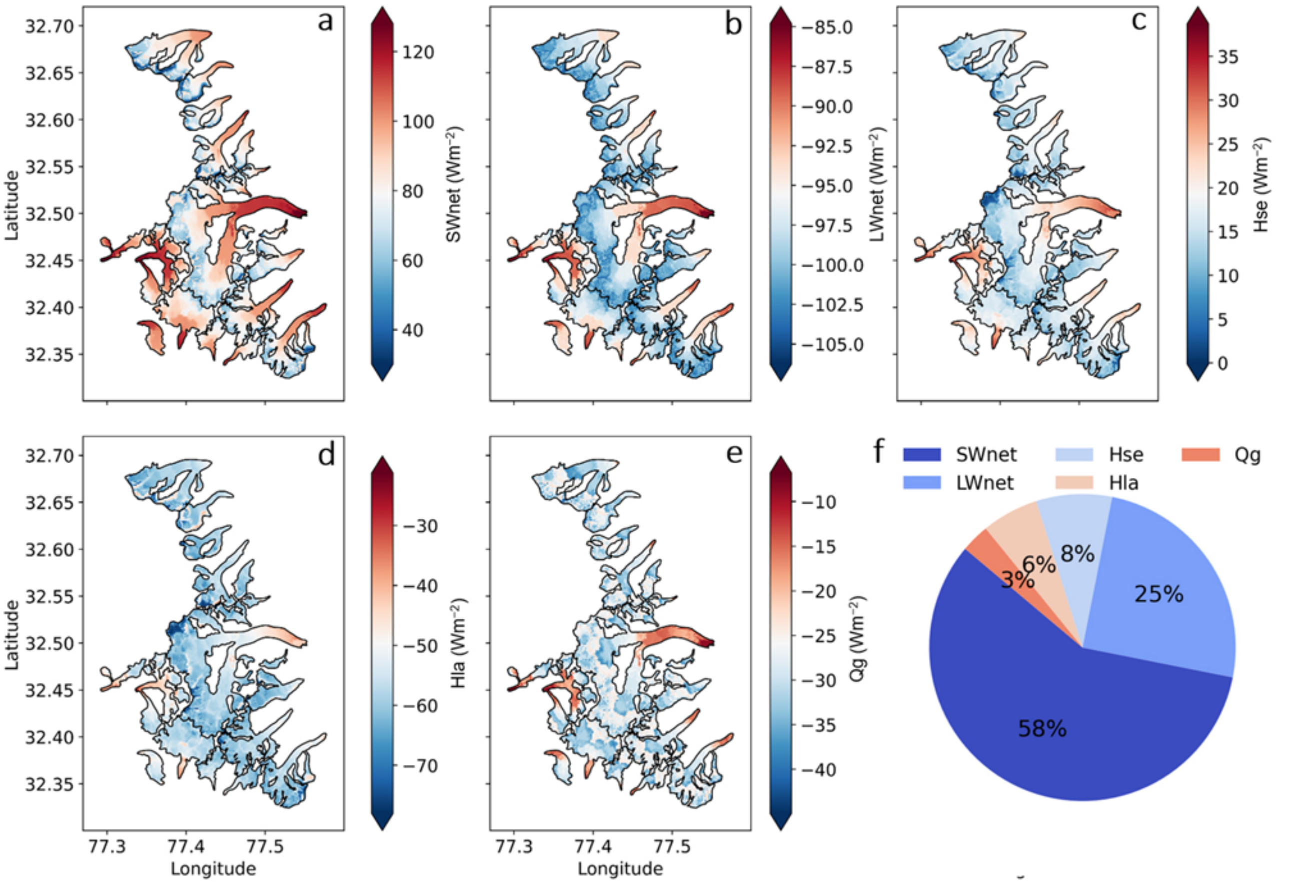

Figure 3. Distributed mean surface energy fluxes for the glaciers of the upper Chandra Basin for the period from October 2015 to September 2022. (a) SW_{net} is net shortwave radiation (Wm^{-2}), (b) LW_{net} is net longwave radiation (Wm^{-2}), (c) H_{se} is sensible heat flux (Wm^{-2}), (d) H_{la} is latent heat flux (Wm^{-2}), (e) Q_g is ground heat flux (Wm^{-2}) and (f) annual contribution of each energy flux in percentage.

mean pressure ranges from 597 to 636 hPa (Fig. 2f). The cloud cover shows strong monthly variation (Fig. 2g). This significant variability in meteorological variables can be attributed to the semi-arid climate conditions prevailing in the area (Bookhagen and Burbank, 2010). During the summer, warm and humid air is brought into the region, causing temperatures to rise (Oulkar, 2022). Consequently, the higher humidity levels also contribute to the warmer climate during this period. In contrast, during the winter, the monsoon winds subside, and the WB becomes active, leading to a drop in temperatures and an increase in cloud cover (Fig. 2a, g). The combined influence of these factors results in the observed variations in the Chandra Basin climate. The variation of temperatures, radiations, wind and moisture throughout the year can affect the ablation and accumulation rates of the glaciers, leading to changes in their overall SMB.

4.2. Distributed surface energy fluxes

The distributed energy fluxes over 7 hydrological years (2015–22), including mean net shortwave (SW_{net}) and longwave (LW_{net}) radiation, mean turbulent heat fluxes (H_{se} and H_{la}) and mean ground heat flux (Q_g), are shown in Fig. 3. The mean SW_{net} ranges from 30 to 130 Wm^{-2} (Fig. 3a) and varies with altitude. Specifically, the SW_{net} values decrease with increasing altitude, primarily due to the higher albedo over the accumulation zone. The SW_{net} is the largest energy source, with higher values in the ablation zone compared to the accumulation zone. This reflects the lower albedo and greater absorbed solar radiation at lower elevations. SW_{net} shows strong seasonal variation, with peak value during the ablation season when incoming solar radiation is at a maximum. The mean LW_{net} varied from −106 to −84 Wm^{-2} and decreased with the altitude (Fig. 3b). This variation can be attributed to the influence of temperature and relative humidity as a function of altitude (Oulkar, 2022). The LW_{net} is negative across the region, indicating radiative cooling. More negative values are found at higher altitudes, likely due to colder temperatures. The turbulent heat flux H_{se} (0–38 Wm^{-2}) and H_{la} (−78 to −21 Wm^{-2}) shows strong spatial variation (Fig. 3c, d). The turbulent heat fluxes of H_{se} and H_{la}, shows maximum values at lower elevations due to the presence of large gradients in surface temperature and water vapour pressure. As altitude increases, the turbulent heat fluxes decrease (Fig. 3c, d). The magnitude of Q_g heat flux is small compared to the other energy components and varied from −44 to −7 Wm^{-2} (Fig. 3e).

The surface energy flux components show a strong seasonality, with net shortwave and longwave radiation being the dominant energy flux in the ablation season (May–September). In contrast, sensible and latent heat flux dominate in the accumulation season (October–April). The annual energy flux analysis showed that the net shortwave radiation contributed 58% to the total surface energy fluxes, followed by net longwave radiation at 25%, sensible heat at

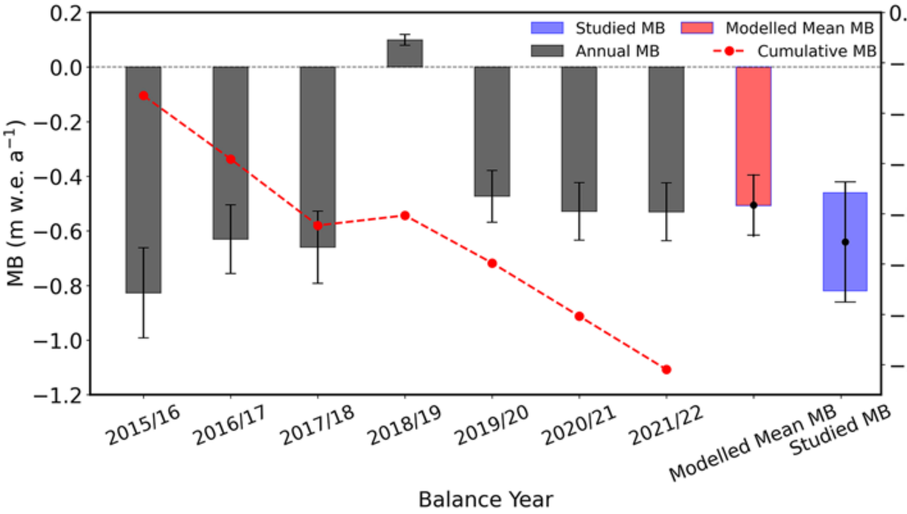

Figure 4. Mean annual mass balance of upper Chandra Basin for 7 hydrological years from October 2015 to September 2022. The red bar is modelled mean mass balance for 7 years, the purple box is previously studied mean mass balance within Chandra Basin (Table 3), and the red line shows the cumulative mass balance.

8%, latent heat at 6% and ground heat flux at 3% (Fig. 3f). These observations are consistent with previous studies on Himalayan glaciers in this region (Azam, 2014b; Patel, 2021; Oulkar, 2022). Also, the altitude dependence and seasonal variations match previous observations on high mountain glaciers (Nair and others, 2023).

4.3. Mass balance

4.3.1. Mean mass balance

Figure 4 shows the changes in the SMB of the upper Chandra Basin over 7 hydrological years from 2015 to 2022. The annual SMB ranges from −0.89 to 0.10 m w.e., indicating an overall trend of negative SMB. The estimated mean SMB of upper Chandra Basin glaciers is −0.51 ± 0.28 m w.e. a^{-1} with a cumulative mass balance of −3.54 m w.e. during the last 7 years. Overall, the modelled mean SMB for 7 hydrological years is consistent with the SMB reported by various studies within the Chandra Basin (Table 3). However, a positive SMB is observed for the hydrological year 2018/19. This could be attributed to higher accumulation driven by an extreme snowfall event in 2018 that covered most of the Lahaul–Spiti district (Pratap, 2023). However, this does not change the overall trend of glacier mass balance, driven by long-term climate change. The modelled result agrees with the general trend of decreasing SMB over time, indicating that the upper Chandra Basin is experiencing glacier mass loss.

4.3.2. Distributed mass balance

Figure 5 highlights the variability of glacier SMB across upper Chandra Basin and shows the glaciers experiencing mass loss in the ablation zone. This study shows spatial variability in SMB, with lower values in the high-elevation areas of the glaciers and higher values in the lower elevation. This spatial variability can be attributed to several factors, including differences in glacier geometry, aspect and shading effects (Yu, 2013; Brun, 2019; Olson and Rupper, 2019; Kumar, 2021; Wang, 2022). Along with meteorological parameters, other variables like precipitation distribution, snowdrift effect, albedo differences and streamflow can also contribute to the spatial SMB variability (Yang, 2013; Brun, 2015).

Table 3. Various methods of mean mass balance for Chandra Basin glaciers

Mass Balance Method	Mean Mass Balance (m w.e. a^{-1})	Year	Reference
Geodetic*	−0.47 ± 0.50	1989–2020	Chandrasekharan and Ramsankaran (2023)
VIC Model*	−0.18 ± 0.14	1980–2018	Laha and others (2023)
Energy balance^{+}	−0.82 ± 0.21	2015–17	Oulkar (2022)
Energy balance^{+}	−0.59 ± 0.12	2013–18	Patel (2021)
Glaciological$^{@}$	−0.57 ± 0.12	2013–17	Sharma and others (2020)
Glaciological$^{\$}$	−0.46 ± 0.40	2002–19	Mandal (2020)
Geodetic*	−0.31 ± 0.08	2000–16	Shean (2020)
Geodetic*	−0.13 ± 0.14	1975–2000	Maurer and others (2019)
Geodetic*	−0.48 ± 0.15	2001–16	Maurer and others (2019)
Geodetic*	−0.30 ± 0.10	2000–15	Mukherjee and others (2018)
Geodetic*	−0.37 ± 0.09	2000–16	Brun and others (2017)
Geodetic*	−0.61 ± 0.46	1984–2012	Tawde and others (2017)
Geodetic*	−0.37 ± 0.09	2000–16	Brun and others (2017)
Glaciological$^{\$}$	−0.56 ± 0.40	2002–14	Azam (2016)
Geodetic*	−0.52 ± 0.32	2000–12	Vijay and Braun (2016)
Geodetic$^{\wedge}$	−1.44 ± 0.69	2001–12	Mishra and others (2014)
Geodetic*	−0.68 ± 0.15	1999–2011	Gardelle and others (2013)
Geodetic*	−0.44 ± 0.09	1999–2011	Vincent (2013)

Region: *Chandra Basin, $^{+}$Sutri Dhaka, $^{\#}$Eight glaciers, $^{@}$Five glaciers, $^{\$}$Chhota Shigri, $^{\wedge}$Hampta.

4.4. Non-climatic parameters and mass-balance spatial variability

The upper Chandra Basin has varying topography, including differences in elevation, size, aspect, orientation and slope, as detailed in Table S2. Higher elevations (>5500 m a.s.l.) have lower temperatures, humidity, air pressure and different precipitation patterns (Bhattacharya, 2023). This leads to more positive or balanced SMB at and above median elevations but increasing negative SMB at lower elevations (Fig. 5a and Table S2 in the Supplementary). For example, glaciers in the study area lost 31% of its SMB within the 4700–5400 m a.s.l. elevation range and remaining SMB loss over lower elevation. Furthermore, higher elevations receive more solid precipitation due to colder temperatures,

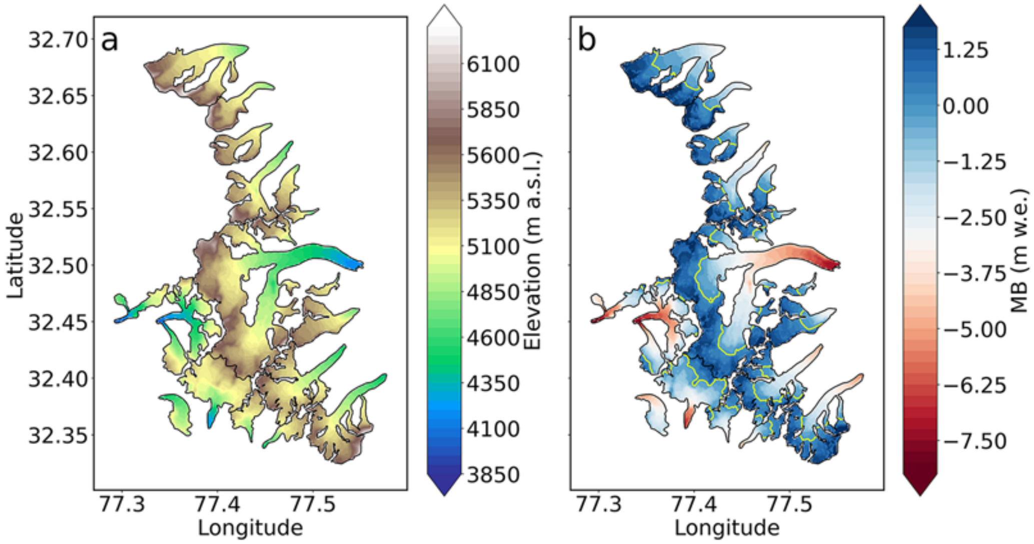

Figure 5. (a) Digital elevation model (DEM) and (b) distributed mean surface mass balance for the glaciers of the upper Chandra Basin for the period from October 2015 to September 2022. The yellow line indicates the equilibrium line altitude (ELA).

resulting in more accumulation (Bhattacharya, 2023). However, meteorological conditions can vary at different elevations at particular seasons, such as the onset or end of summer when snowfall may occur in upper accumulation zones while melt continues in lower ablation zones (Cuffey and Paterson, 2010). The size and shape of a glacier influence its SMB by affecting accumulation and ablation patterns. For example, the larger Samudra Tapu Glacier had a more negative SMB compared to a smaller glacier (Fig. 5b). Figure 5 depicts that the glaciers with more extensive area coverage at higher elevations are likely to accumulate more mass from solid precipitation, while glaciers with greater area at lower elevations may experience higher ablation rates due to warmer temperatures (Racoviteanu and others, 2015).

Furthermore, our results indicate that southeast, south, southwest and west-facing aspects correspond to the zones with the highest average rates of ablation in the study area (Figs. 5b and 6a). This is likely due to the effects of topographic shading on spatial variability in SMB. Glaciers on northeast-facing slopes receive less direct solar radiation, and experience reduced ablation compared to southwest-facing glaciers (Figs. 5b and 6a), which is consistent with findings by Olson and Rupper (2019). Mountain shadows can partially cover glaciers, limiting sunlight exposure and reducing melting, which is in agreement with previous studies (Klok and Oerlemans, 2002; Wang, 2022). Topographic shading directly alters the radiation budget at the glacier surface by obstructing incoming solar radiation (Olson and Rupper, 2019; Wang, 2022; Zhang and others, 2024). Our results indicate that topographic shading plays a crucial role in controlling SEB and SMB estimates.

The slope of selected glaciers in the upper Chandra Basin ranges from 1° to 57° with a mean of 15° (Fig. 6b and Table S2 in the Supplementary). However, the majority of the glacier area in the study region has a gentle slope of 12–20° (Fig. 6b and Table S2 in the Supplementary). These moderate-slope zones, comprising most of the glacier area, experience the highest melting rates, agreeing with other findings (Fischer and others, 2015; Rabatel and others, 2016; Kumar, 2021). In the lower ablation zone of a glacier, the slope is gentle, resulting in a low-temperature gradient in most parts of the Himalaya (Zhang and others, 2022). Consequently, this area experiences higher rates of melting. In contrast, the accumulation zone of the glacier has a steeper slope, leading to a higher temperature gradient and lower rates of melting across the High Mountain Asia glaciers (Zhang and others, 2022). The steep slopes in upper accumulation zones are less susceptible to regional mass loss (Fischer and others, 2015; Rabatel and others, 2016; Davaze and others, 2020; Kumar, 2021). More gentle slopes correlate with more negative SMB over lower ablation zones, as also reported by Davaze and others (2020) for glaciers in the European Alps.

We find that the aspect, slope, size and elevation of the glacier contribute towards the spatial variability of SMB within the study region, consistent with previous studies that have examined the complex relationship between topography and glacier melt dynamics.

4.5. Glaciers mass-balance sensitivity to climatic conditions

Variations in air temperature and precipitation play pivotal roles in driving glacier SMB changes, as explored through simulations conducted to investigate their impact on the SMB of the Sutri Dhaka Glacier (Oulkar, 2022). Therefore, to evaluate the climate sensitivity of the upper Chandra Basin glacier SMB, perturbation experiments of air temperature and precipitation are performed. During these simulations, other pertinent variables (incoming shortwave radiation, incoming longwave radiation, relative humidity, surface pressure, wind speed and cloud cover) remained constant. Additionally, a coupled parameter perturbation approach is employed, wherein alterations in both air temperature and precipitation are simultaneously introduced as forcings to the model. This approach mainly sought to address the extent to which changes in precipitation could compensate for the additional loss of glacier mass attributed to a 1°C increase in air temperature.

To simulate temperature variations, we changed the air temperature by a step of 0.5°C from −2°C to +2°C while keeping other input parameters constant (Fig. 7). The results show that a temperature increase of 1°C led to a 64% reduction in the total SMB (an increase in mass loss from mean SMB). In contrast, a temperature decrease of 1°C resulted in a 51% increase in the SMB (a decrease in mass loss) (Fig. 7). Moreover, when the temperature is increased

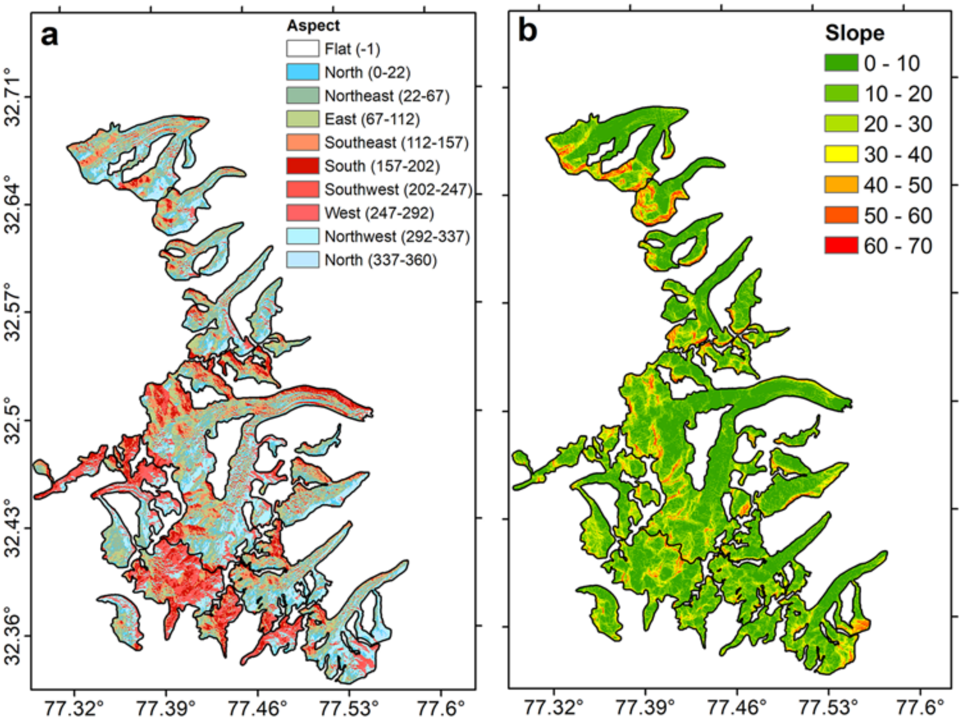

Figure 6. The upper Chandra Basin map showing (a) aspect, (b) slope.

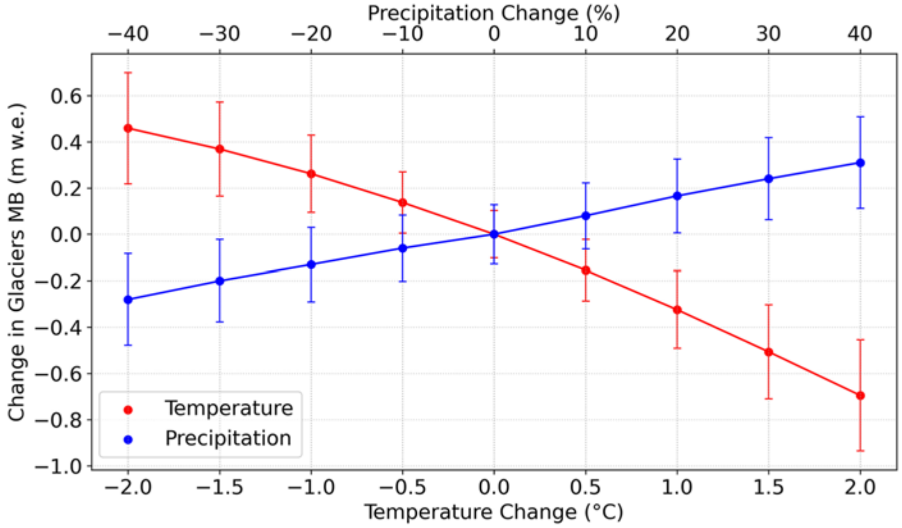

Figure 7. Sensitivity of mass balance in the upper Chandra Basin glaciers to air temperature and precipitation changes.

by 2°C, the total SMB decreases by 136%. In contrast, a temperature decrease of 2°C led to a 90% increase in the total SMB. Similarly, we conducted the simulations to explore the effects of precipitation changes using eight scenarios, where the precipitation is adjusted in 10% increments from −40% to +40%. Increasing the precipitation by 20% resulted in a 32% increase in the total SMB, while a 20% decrease led to a 25% reduction in the total SMB. Notably, at a 40% increase in precipitation, the total SMB exhibited a slightly less negative equivalent to a 60% increase in glacier SMB.

Further, the temperature and precipitation have different elevation gradient, indicating that temperature and precipitation have different effects on glacier SMB (Fig. 7). Notably, augmenting precipitation yields a slightly positive effect compared to reducing precipitation (Fig. 7). Across the upper Chandra Basin, the mass-balance sensitivity for air temperature and precipitation change is −0.29 m w.e. a^{-1} °C^{-1} and 0.14 m w.e. a^{-1} (10%)$^{-1}$, respectively. However, the impact of temperature changes on glacier SMB is more pronounced than that of precipitation changes, as the temperature shows a steeper gradient in comparison to the precipitation (Fig. 7). This is consistent with the findings of previous studies that have shown that temperature is the dominant factor controlling glacier SMB globally (Azam, 2018; Singh and others, 2018; Fugger, 2022). However, precipitation can still influence glacier SMB by affecting the amount and type of precipitation, snowpack density, albedo and run-off. Furthermore, it is observed that higher air temperatures accelerated the rate of glacier mass loss, while the compensatory effect of increased precipitation for change in glacier SMB is gradually limited (Fig.

7). Our findings reveal that a 42% increase in precipitation is necessary to counteract the additional mass loss resulting from a 1°C increase in air temperature for the upper Chandra Basin glaciers.

5. Conclusions

We investigated the distributed SEB and SMB of glaciers in the upper Chandra Basin of the western Himalaya, using a physically based COSIPY model, to estimate energy fluxes and SMB for the Chandra Basin glaciers for 7 hydrological years from 2015 to 2022. Meteorological data from HBC AWS and bias-corrected ERA5 data are employed as input for the model, and the parameters are calibrated using in situ observations. The study addressed uncertainties inherent in the modelling processes through a Monte Carlo simulation approach. The study highlighted the strong seasonality of energy fluxes, with net radiation being the dominant energy flux during summer months, while sensible and latent heat fluxes dominated in the winter. The results also revealed the spatial variability in energy fluxes and SMB across the glaciers within the upper Chandra Basin, highlighting the additional influence of factors like glacier geometry, shading effects, local topography and orientations/aspects. The estimated SMB of the upper Chandra Basin glaciers indicated an overall negative mean annual SMB of -0.51 ± 0.28 m w.e. a^{-1} over the 7 year period. This underscored the impact of climate change on glacier mass loss in the region. Our study demonstrated that the glacier SMB is highly sensitive to changes in air temperature and precipitation, with even small temperature variations causing significant shifts in the SMB. The findings reveal that a 42% increase in precipitation is necessary to counteract the additional mass loss resulting from a 1°C increase in air temperature in the region. The comparison of model results with other SMB studies indicated consistency with the model output and validated the accuracy of the model employed. Our study offers a well-constrained distributed energy and mass balance of glaciers in the upper Chandra Basin and can be used to better understand the impacts of climate variability on the SMB of Himalayan glaciers.

Supplementary material. The supplementary material for this article can be found at 10.1017/aog.2024.46.

Data availability statement. The data used in this analysis are freely available at the National Centre for Polar and Ocean Research (NCPOR) data repository. Himansh Base Camp (HBC) AWS data is available at https://data.ncpor.res.in/static/datasets/him/1_himansh_station_aws_4052.xlsx and point mass balance for Sutri Dhaka and Samudra Tapu Glacier is available at https://data.ncpor.res.in/static/datasets/him/2_Glaciological_Mass_Balance_2015_22.xlsx.

Acknowledgements. We are thankful to National Centre for Polar and Ocean Research (NCPOR) for supporting the research at NCPOR. We are thankful to our field support team who were involved in our field trips. This is NCPOR contribution number J-43/2024-25.

Author contributions. SNO, PS and MT defined the objectives and designed the study. SNO, PS, BP, LKP and ATS collected the automatic weather station and in situ mass-balance data. SNO conducted an analysis and wrote the article, with contributions from PS, SL, BP and MT. All authors contributed to the discussion of the article.

Funding statement. We thank the Ministry of Earth Sciences for financial support through the project "PACER—Cryosphere and Climate."

Competing interests. The authors declare no competing interests.

References

Arndt A and Schneider C (2023) Spatial pattern of glacier mass balance sensitivity to atmospheric forcing in High Mountain Asia. *Journal of Glaciology*. doi: 10.1017/jog.2023.46

Azam MF and 6 others (2014b) Processes governing the mass balance of Chhota Shigri Glacier (western Himalaya, India) assessed by point-scale surface energy balance measurements. *Cryosphere* **8**(6), 2195–2217. doi: 10.5194/tc-8-2195-2014

Azam MF and 10 others (2016) Meteorological conditions, seasonal and annual mass balances of Chhota Shigri Glacier, western Himalaya, India. *Annals of Glaciology* **57**(71), 328–338. doi: 10.3189/2016AoG71A570

Azam MF and 5 others (2018) Review of the status and mass changes of Himalayan-Karakoram glaciers. *Journal of Glaciology* **64**(243), 61–74. doi: 10.1017/jog.2017.86

Azam MF and 12 others (2021) Glaciohydrology of the Himalaya-Karakoram. *Science* **373**(6557), 869–+. doi: 10.1126/science.abf3668

Bhattacharya A and 6 others (2023) Influence of climate and non-climatic attributes on declining glacier mass budget and surging in Alaknanda Basin and its surroundings. *Global and Planetary Change*, 230. doi: 10.1016/j.gloplacha.2023.104260

Bolch T and 11 others (2012) The state and fate of Himalayan glaciers. *Science* **336**(6079), 310–314. doi: 10.1126/science.1215828

Bookhagen B and Burbank DW (2010) Toward a complete Himalayan hydrological budget: Spatiotemporal distribution of snowmelt and rainfall and their impact on river discharge. *Journal of Geophysical Research-Earth Surface*, 115. doi: 10.1029/2009jf001426

Brun F and 8 others (2015) Seasonal changes in surface albedo of Himalayan glaciers from MODIS data and links with the annual mass balance. *The Cryosphere* **9**(1), 341–355. doi: 10.5194/tc-9-341-2015

Brun F and 6 others (2019) Heterogeneous influence of glacier morphology on the mass balance variability in High Mountain Asia. *Journal of Geophysical Research-Earth Surface* **124**(6), 1331–1345. doi: 10.1029/2018jf004838

Brun F, Berthier E, Wagnon P, Kaab A, and Treichler D (2017) A spatially resolved estimate of High Mountain Asia glacier mass balances from 2000 to 2016. *Nature Geoscience* **10**(9), 668–673. doi: 10.1038/ngeo2999

Chandrasekharan A and Ramsankaran R (2023) Reconstructing 32 years (1989-2020) of annual glacier surface mass balance in Chandra Basin, Western Himalayas, India. *Regional Environmental Change* **23**(4). doi: 10.1007/s10113-023-02112-4

Cuffey KM and Paterson WSB (2010) *The Physics of Glaciers*. London, UK: Academic Press.

Davaze L, Rabatel A, Dufour A, Hugonnet R and Arnaud Y (2020) Region-wide annual glacier surface mass balance for the European Alps from 2000 to 2016. *Frontiers in Earth Science*, 8. doi: 10.3389/feart.2020.00149

Estévez J, Gavilán P and Giráldez JV (2011) Guidelines on validation procedures for meteorological data from automatic weather stations. *Journal of Hydrology* **402**(1-2), 144–154. doi: 10.1016/j.jhydrol.2011.02.031

Fischer M, Huss M and Hoelzle M (2015) Surface elevation and mass changes of all Swiss glaciers 1980-2010. *Cryosphere* **9**(2), 525–540. doi: 10.5194/tc-9-525-2015

Fugger S and 11 others (2022) Understanding monsoon controls on the energy and mass balance of glaciers in the Central and Eastern Himalaya. *The Cryosphere* **16**(5), 1631–1652. doi: 10.5194/tc-16-1631-2022

Gardelle J, Berthier E, Arnaud Y and Kaab A (2013) Corrigendum to "Region-wide glacier mass balances over the Pamir-Karakoram-Himalaya during 1999–2011" published in The Cryosphere, 7, 1263–1286, 2013. *The Cryosphere* **7**(6), 1885–1886. doi: 10.5194/tc-7-1885-2013

Georg W, Albin H, Georg N, Katharina S, Enrico T and Peng Z (2016) On the energy balance closure and net radiation in complex terrain. *Agricultural and Forest Meteorology* **226**, 37–49. doi: 10.1016/j.agrformet.2016.05.012

Hersbach H and 42 others (2020) The ERA5 global reanalysis. *Quarterly Journal of the Royal Meteorological Society* **146**(730), 1999–2049. doi: 10.1002/qj.3803

Hock R and 6 others (2019) IPCC Special Report on the Ocean and Cryosphere in a Changing Climate, Chap 2, in High mountain areas. (eds. Pörtner H-O **and others**), 131–202.

Hock R and Holmgren B (2005) A distributed surface energy-balance model for complex topography and its application to Storglaciaren, Sweden. *Journal of Glaciology* **51**(172), 25–36. doi: 10.3189/172756505781829566

Huintjes E and 9 others (2015) Evaluation of a coupled snow and energy balance model for Zhadang glacier, Tibetan Plateau, using glaciological measurements and time-lapse photography. *Arctic Antarctic and Alpine Research* **47**(3), 573–590. doi: 10.1657/aaar0014-073

Immerzeel WW and 31 others (2020) Importance and vulnerability of the world's water towers. *Nature* **577**(7790), 364–369. doi: 10.1038/s41586-019-1822-y

Kaab A, Berthier E, Nuth C, Gardelle J and Arnaud Y (2012) Contrasting patterns of early twenty-first-century glacier mass change in the Himalayas. *Nature* **488**(7412), 495–498. doi: 10.1038/nature11324

Klok EJ and Oerlemans J (2002) Model study of the spatial distribution of the energy and mass balance of Morteratschgletscher, Switzerland. *Journal of Glaciology* **48**(163), 505–518. doi: 10.3189/172756502781831133

Koul MN and Ganjoo RK (2010) Impact of inter- and intra-annual variation in weather parameters on mass balance and equilibrium line altitude of Naradu Glacier (Himachal Pradesh), NW Himalaya, India. *Climatic Change.* **99**(1), 119–139. doi: 10.1007/s10584-009-9660-9

Kulkarni AV and 6 others (2007) Glacial retreat in Himalaya using Indian Remote Sensing satellite data. *Current Science* **92**(1), 69–74. jstor.org/stable/24096824

Kumar R and 5 others (2021) Surface mass balance analysis at Naradu Glacier, Western Himalaya, India. *Scientific Reports* **11**(1). doi: 10.1038/s41598-021-91348-3

Laha S, Banerjee A, Singh A, Sharma P and Thamban M (2023) Climate sensitivity of the summer runoff of two glacierised Himalayan catchments with contrasting climate. *Hydrology and Earth System Sciences* **27**(2), 627–645. doi: 10.5194/hess-27-627-2023

Li XY and 7 others (2022) Climate change threatens terrestrial water storage over the Tibetan Plateau. *Nature Climate Change* **12**(9), 801–807. doi: 10.1038/s41558-022-01443-0

Machguth H, Purves RS, Oerlemans J, Hoelzle M and Paul F (2008) Exploring uncertainty in glacier mass balance modelling with Monte Carlo simulation. *The Cryosphere* **2**(2), 191–204. doi: 10.5194/tc-2-191-2008

Mandal A and 9 others (2020) Understanding the interrelationships among mass balance, meteorology, discharge and surface velocity on Chhota Shigri Glacier over 2002-2019 using in situ measurements. *Journal of Glaciology* **66**(259), 727–741. doi: 10.1017/jog.2020.42

Maraun D and Widmann M (2018) In *Statistical Downscaling and Bias Correction for Climate Research*. Cambridge: Cambridge University Press, 303–341.

Maurer JM, Schaefer JM, Rupper S and Corley A (2019) Acceleration of ice loss across the Himalayas over the past 40 years. *Science Advances* **5**(6). doi: 10.1126/sciadv.aav7266

Mayewski PA, Perry LB, Matthews T and Birkel SD (2020) Climate Change in the Hindu Kush Himalayas: Basis and Gaps. *One Earth* **3**(5), 551–555. doi: 10.1016/j.oneear.2020.10.007

Mishra R, Kumar A and Singh D (2014) Long term monitoring of mass balance of Hamtah Glacier, Lahaul and Spiti district, Himachal Pradesh. *Geological Survey of India* **147**(pt 8), 230–231.

Molg T and Scherer D (2012) Retrieving important mass-balance model parameters from AWS measurements and high-resolution mesoscale atmospheric modeling. *Journal of Glaciology* **58**(209), 625–628. doi: 10.3189/2012JoG11J258

Mukherjee K, Bhattacharya A, Pieczonka T, Ghosh S and Bolch T (2018) Glacier mass budget and climate reanalysis data indicate a climatic shift around 2000 in Lahaul-Spiti, western Himalaya. *Climatic Change* **148**(1-2), 219–233. doi: 10.1007/s10584-018-2185-3

Nair VS, Usha KH and Suresh Babu S (2023) Elevation-dependence of warming due to aerosol-induced snow darkening over the Himalayan-Tibetan region. *Environmental Research Letters*, 19. doi: 10.1088/1748-9326/ad1346

Oerlemans J (2001) In *Glaciers and Climate Change*. Lisse: Swets & Zeitlinger, 148pp.

Oerlemans J and Knap WH (1998) A 1 year record of global radiation and albedo in the ablation zone of Morteratschgletscher, Switzerland. *Journal of Glaciology* **44**(147), 231–238. doi: 10.3189/s0022143000002574

Olson M and Rupper S (2019) Impacts of topographic shading on direct solar radiation for valley glaciers in complex topography. *The Cryosphere* **13**(1), 29–40. doi: 10.5194/tc-13-29-2019

Oulkar SN and 7 others (2022) Energy fluxes, mass balance, and climate sensitivity of the Sutri Dhaka Glacier in the western Himalaya. *Frontiers in Earth Science*, 10. doi: 10.3389/feart.2022.949735

Patel A and 6 others (2021) Estimation of mass and energy balance of glaciers using a distributed energy balance model over the Chandra river basin (Western Himalaya). *Hydrological Processes*. doi: 10.1002/hyp.14058

Pepin NC and 13 others (2022) Climate changes and their elevational patterns in the mountains of the world. *Reviews of Geophysics* **60**(1). doi: 10.1029/2020rg000730

Pratap B and 5 others (2023) Differential surface melting of a debris-covered glacier and its geomorphological control - A case study from Batal Glacier, western Himalaya. *Geomorphology*, 431. doi: 10.1016/j.geomorph.2023.108686

Pratap B, Sharma P, Patel L, Singh A T, Gaddam V Kumar, Oulkar S and Thamban M (2019) Reconciling High Glacier Surface Melting in Summer with Air Temperature in the Semi-Arid Zone of Western Himalaya. Water, **11**(8), 1561. doi: 10.3390/w11081561

Pritchard HD (2019) Asia's shrinking glaciers protect large populations from drought stress. *Nature* **569**(7758), 649–654. doi: 10.1038/s41586-019-1240-1

Rabatel A, Dedieu JP and Vincent C (2016) Spatio-temporal changes in glacier-wide mass balance quantified, by optical remote sensing on 30 glaciers in the French Alps for the period 1983-2014. *Journal of Glaciology* **62**(236), 1153–1166. doi: 10.1017/jog.2016.113

Racoviteanu AE, Arnaud Y, Williams MW and Manley WF (2015) Spatial patterns in glacier characteristics and area changes from 1962 to 2006 in the Kanchenjunga-Sikkim area, eastern Himalaya. *The Cryosphere* **9**(2), 505–523. doi: 10.5194/tc-9-505-2015

Reijmer CH, van den Broeke MR, Fettweis X, Ettema J and Stap LB (2012) Refreezing on the Greenland ice sheet: A comparison of parameterizations. *The Cryosphere* **6**(4), 743–762. doi: 10.5194/tc-6-743-2012

Sakai A and Fujita K (2017) Contrasting glacier responses to recent climate change in high-mountain Asia. *Scientific Reports* **7**, 8. doi: 10.1038/s41598-017-14256-5

Sauter T, Arndt A and Schneider C (2020) COSIPY v1.3-an open-source coupled snowpack and ice surface energy and mass balance model. *Geoscientific Model Development* **13**(11), 5645–5662. doi: 10.5194/gmd-13-5645-2020

Sharma P, Patel LK, Singh AT, Meloth T and Ravindra R (2020) Glacier response to climate in Arctic and Himalaya during last seventeen years: A case study of Svalbard, Arctic and Chandra Basin, Himalaya. In Goel PS, Ravindra R and Chattopadhyay S (eds), *Climate Change and the White World*. Cham, Switzerland: Springer, 139–156.

Shean DE and 5 others (2020) A systematic, regional assessment of High Mountain Asia Glacier Mass Balance. *Frontiers in Earth Science* **7**. doi: 10.3389/feart.2019.00363

Singh S, Kumar R and Dimri AP (2018) Mass balance status of Indian Himalayan Glaciers: A brief review. *Frontiers in Environmental Science*, 6. doi: 10.3389/fenvs.2018.00030

Tachikawa T (2011) Characteristics of ASTER GDEM version 2. *IEEE International Geoscience and Remote Sensing Symposium*, 3657–3660. doi: 10.1109/IGARSS.2011.6050017.

Tawde SA, Kulkarni AV and Bala G (2017) An estimate of glacier mass balance for the Chandra basin, western Himalaya, for the period 1984-2012. *Annals of Glaciology* **58**(75), 99–109. doi: 10.1017/aog.2017.18

Van den Broeke M, Reijmer C, Van As D and Boot W (2006) Daily cycle of the surface energy balance in Antarctica and the influence of clouds. *International Journal of Climatology* **26**(12), 1587–1605. doi: 10.1002/joc.1323

van der Veen CJ (2002) Polar ice sheets and global sea level: How well can we predict the future? *Global and Planetary Change* **32**(2-3), 165–194. doi: 10.1016/s0921-8181(01)00140-0

Vijay S and Braun M (2016) Elevation Change Rates of Glaciers in the Lahaul-Spiti (Western Himalaya, India) during 2000-2012 and 2012-2013. *Remote Sensing* **8**(12). doi: 10.3390/rs8121038

Vincent C and 10 others (2013) Balanced conditions or slight mass gain of glaciers in the Lahaul and Spiti region (northern India, Himalaya) during the nineties preceded recent mass loss. *Cryosphere* **7**(2), 569–582. doi: 10.5194/tc-7-569-2013

Wang RJ and 6 others (2022) Influence of topographic shading on the mass balance of the High Mountain Asia Glaciers. *Remote Sensing* **14**(7). doi: 10.3390/rs14071576

Wang SJ, Zhang MJ, Wang BL, Sun MP and Li XF (2013) Recent changes in daily extremes of temperature and precipitation over the western Tibetan Plateau, 1973-2011. *Quaternary International* **313**, 110–117. doi: 10.1016/j.quaint.2013.03.037

Yang W and 5 others (2013) Mass balance of a maritime glacier on the southeast Tibetan Plateau and its climatic sensitivity. *Journal of Geophysical Research: Atmospheres* **118**(17), 9579–9594. doi: 10.1002/jgrd.50760

Yu W and 10s others (2013) Different region climate regimes and topography affect the changes in area and mass balance of glaciers on the north and south slopes of the same glacierized massif (the West Nyainqentanglha Range, Tibetan Plateau). *Journal of Hydrology* **495**, 64–73. doi: 10.1016/j.jhydrol.2013.04.034

Zhang YL, Li X, Chang XL, Luo DL, Wang X and Cheng GD (2024) Impacts of topographic shadows cast by surrounding terrain on the solar irradiance on glaciers' surface in High Mountain Asia (HMA). *Atmospheric Research*, 307. doi: 10.1016/j.atmosres.2024.107511

Zhang Z, Gu ZN, Hu KH, Xu YY and Zhao JB (2022) Spatial variability between glacier mass balance and environmental factors in the High Mountain Asia. *Journal of Arid Land* **14**(4), 441–454. doi: 10.1007/s40333-017-0014-z